

Numerical approach for Corvino-type gluing of Brill–Lindquist initial data

Daniel Pook-Kolb^{1,2} and Domenico Giulini^{3,4} 

¹ Max Planck Institute for Gravitational Physics (Albert Einstein Institute), Callinstrasse 38, D-30167 Hannover, Germany

² Leibniz Universität Hannover, 30167 Hannover, Germany

³ Institute for Theoretical Physics, Leibniz Universität Hannover, Appelstrasse 2, D-30167 Hannover, Germany

⁴ Center of Applied Space Technology and Microgravity, University of Bremen, Am Fallturm 1, D-28359 Bremen, Germany

E-mail: daniel.pook.kolb@aei.mpg.de and domenico.giulini@itp.uni-hannover.de

Received 10 September 2018, revised 19 November 2018

Accepted for publication 16 January 2019

Published 31 January 2019



CrossMark

Abstract

Building on the work of Giulini and Holzegel (2005 (arXiv:gr-qc/0508070)), a new numerical approach is developed for computing Cauchy data for Einstein's equations by *gluing* a Schwarzschild end to a Brill–Lindquist metric via a Corvino-type construction. In contrast to, and in extension of, the numerical strategy of Doulis and Rinne (2016 *Class. Quantum Grav.* **33** 075014), the overdetermined Poisson problem resulting from the Brill wave ansatz is decomposed to obtain two uniquely solvable problems. A pseudospectral method and a Newton–Krylov root finder are utilized to perform the gluing. The convergence analysis strongly indicates that the numerical strategy developed here is able to produce highly accurate results. It is observed that Schwarzschild ends of various ADM masses can be glued to the same interior configuration using the same gluing radius.

Keywords: general relativity, numerical relativity, initial-value problem

(Some figures may appear in colour only in the online journal)

1. Introduction

The theoretical possibility of gravitational-wave generation through the merger of two black holes has recently received spectacular confirmation through several earth-bound detections of gravitational waves by the LIGO–Virgo–Collaboration [1–3]. Also, these observations were most recently complemented by the no less spectacular detection of the gravitational-wave signal from the merger of two neutron-stars [4]. From a theoretical point of view the problem



of modelling binary neutron-star systems differs drastically from the former insofar as it involves a complicated coupled system of differential equations that governs both, the dynamics of the gravitational field and that of the neutron matter composing the stars. In contrast, the theoretical analysis of the dynamics of black holes ‘only’ involves the sourceless (i.e. vacuum) Einstein equations of general relativity. Hence, in terms of differential equations, black holes pose the much ‘cleaner’ problem.

But even in this ‘simpler’ case there are still unresolved mathematical issues of undeniable physical relevance in connection with the initial-value formulation of the matter-free field equations of general relativity. We recall that these are ten coupled non-linear but quasi-linear partial differential equations of second order for the ten components $g_{\mu\nu}$ of the space-time metric. Here, as usual, Greek indices range in the set $\{0, 1, 2, 3\}$ and for definiteness we state that we use the ‘mostly-plus’ convention concerning the signature, though this will be irrelevant for the rest of this paper. This system of differential equations can be cast into the form of a Hamiltonian system (see, e.g. [5]) which reveals its hybrid-nature in the following sense. Six out of the ten equations are of (underdetermined) hyperbolic type and hence comprise the evolutionary content of Einstein’s equations, whereas the remaining four equations are of (underdetermined) elliptic type. The latter are constraints in the sense that they only involve the initial data and their spatial derivatives, but not their time derivatives. Hence they properly constrain the initial data themselves, rather than their evolution. In this paper we will be exclusively concerned with these constraints.

There exists a considerably large body of knowledge concerning explicit analytic expressions of solutions to the constraints representing initial data for two or more black holes. A classic paper is [6], in which initial data are given for two black holes without orbital and spin angular momentum at the moment of rest. For such ‘time symmetric initial data’ (vanishing linear and angular momenta), and under the assumption that the Cauchy hypersurface is conformally flat, the constraints simply reduce to a single Laplace equation for the conformal factor; see, e.g. [5] for a review. Hence a whole arsenal of techniques, like Thomson’s method of images familiar from electrostatics, can be employed to construct solutions with various kinds of symmetries [7], even in the time-asymmetric case; e.g. [8, 9]. A modern comprehensive reference explaining and comparing the various methods for general-data building is [10].

However, there is one physical issue that affects all these data alike, even the most simple ones, which usually goes under the name of ‘spurious’ or ‘junk’ radiation; compare, e.g. [11], section 3.2.3⁵. That is to say, all these data already contain initial gravitational radiation that fills space up to infinity, as depicted in our figure 1. That radiation is clearly seen in numerical simulations, e.g. [12], and needs to be distinguished and separated from that radiation that is dynamically produced by the process of black-hole collision. Usually this is pragmatically done by simply ignoring the radiation that identifies itself as being ‘spurious’—in the sense of *not* being produced in the scattering and merging process—by arriving too early at large spatial distances, that is, outside the causal future of the merging event; compare again figure 1. But for general data it cannot be expected that spurious and proper radiation will always emerge as two sufficiently localised and separated packages in time. A lack of separability will clearly introduce uncertainties in the calculation of dynamically sourced radiation energy. This happened, e.g. for the (non time-symmetric) Kerr–Schild data studied in [12]. Again in the non time-symmetric case it was observed in [13] that spurious radiation could be removed from the Bowen–York data [8] for spinning black holes by modification of the extrinsic curvatures, keeping however conformal flatness of the metric. As far as we are aware, there is no systematic insight connected with this observation. This also holds for the

⁵ In what follows we shall regard both terms, ‘spurious’ and ‘junk’, synonymously, but shall mostly use ‘spurious’.

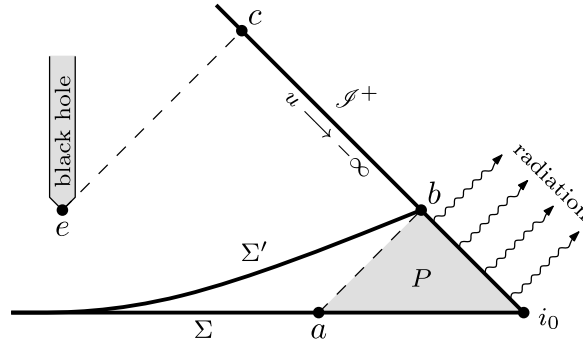


Figure 1. Conformal (Penrose) diagram of spacetime with two spacelike hypersurfaces Σ and Σ' ending at spacelike infinity i_0 and future lightlike infinity \mathcal{S}^+ , respectively. Σ depicts an asymptotically flat Cauchy surface, whereas Σ' is asymptotically hyperboloidal and not Cauchy. u denotes the standard Bondi parameter along the null generators of \mathcal{S}^+ . The difference between the ADM-mass of Σ (computed at i_0) and the Bondi mass of Σ' (computed at the intersection two-sphere between Σ' and \mathcal{S}^+ , here denoted by the point b) must be due to gravitational radiation escaping between i_0 and b . This radiation originates from the causal past P of the region $\overline{i_0 b} \subset \mathcal{S}^+$, whose intersection with Σ is the region $\overline{a i_0}$. In this sense we say that the data on Σ contain radiation in that region. Any gravitational radiation emerging from an (quasi localised) event e , e.g. the formation of a black hole due to a binary merger, cannot reach \mathcal{S}^+ before the intersection c of the future light-cone at e with \mathcal{S}^+ . In that sense, any radiation reaching \mathcal{S}^+ before c , like that explicitly shown in the figure, is considered ‘junk’ or ‘spurious’.

suggestion made in [11] to the effect that for non time-symmetric data it is conformal flatness that can be held responsible for such excess radiation. This was partially confirmed in [14], where admittance of conformal curvature was numerically observed to result in a 50% reduction. A possible way to understand why this could be the case may be contained in the geometric analysis of the behaviour of marginally outer trapped surfaces of individual holes *after* merging as given in [15], but this is presently also unclear. Only in some rare cases will intuition let us see more or less obvious physical reasons for spurious radiation due to initial data that more or less obviously mismatch the physical proper dynamical situation but which we nevertheless choose due to convenience. This happens, e.g. when we require the initial data of an orbiting binary system to start off with spatially closed orbits corresponding to a spacetime helical symmetry. This will be a good approximation for systems whose components are far apart. For close components, however, for which previous radiation reaction has already left its traces, the orbit is already an inspiraling one rather than perfectly circular at the moment we start to run the initial-value problem. Assuming circularity will then lead to spurious orbit eccentricities which, in turn, radiate off and give rise to what in this context has to count as spurious. See, e.g. chapter 9.4. of [10] and references therein.

All this puts into evidence that current pragmatic procedures, albeit efficient for many of the data sets of interest, are not entirely satisfying from a theoretical and conceptual point of view, where a proper theoretical understanding would certainly be much preferred against a case-to-case prescription based on no better insight than trial and error. Hence the question arises of how to systematically modify the known multi-black-hole initial data sets, so as to remove the spurious radiation while keeping the other aspects intact, like the presence of black holes, their masses, mutual distances, and possible other parameters. This is the question addressed in this paper for the most simple case of the time-symmetric Brill–Lindquist two-hole data [6].

Analytically, the existence of initial gravitational radiation that spreads all the way to infinity has been shown in [16] to relate to the Newman–Penrose constants [17] in case of time-symmetric and conformally flat initial data sets. An explicit calculation performed in [16] showed that the Bondi mass m_{Bondi} can be expressed in terms of the ADM mass m_{ADM} and the five (generally complex-valued) Newman–Penrose constants $G_{-2}, G_{-1}, G_0, G_1, G_2$ as follows:

$$m_{\text{Bondi}} = m_{\text{ADM}} + \sum_{k=-2}^{k=2} |G_k|^2 \left(\frac{\sqrt{2}}{u} \right)^7 + \mathcal{O}(1/u^8). \quad (1)$$

Here u is the Bondi parameter (affine parameter along the null generators of future light-like infinity \mathcal{I}^+) with $u \rightarrow -\infty$ approaching spacelike infinity i_0 ; compare again figure 1. Note that the Bondi mass coincides with the ADM mass at i_0 , i.e. for $u = -\infty$, as it must be, and lies below the latter for finite negative values of u , i.e. in a neighbourhood of i_0 on \mathcal{I}^+ , corresponding to outgoing gravitational radiation. To leading order the Bondi mass is monotonically decreasing in any neighbourhood of i_0 in \mathcal{I}^+ , whereas the ADM mass is a proper geometric invariant of the 3-manifold Σ with asymptotically flat end at i_0 [18].

Furthermore, it has been shown by the same author in [19] that non-vanishing Newman–Penrose constants impose obstructions to smoothness in the transition from spatial infinity (i_0) to null infinity (\mathcal{I}^\pm). It has even been conjectured in [19] that such a smooth transition requires the (time symmetric and conformally flat) data to be *exactly* Schwarzschild in a neighbourhood of i_0 , though recent work [20] on spacetimes admitting polyhomogeneous expansions of the metric at infinity (spacelike and null) suggests that the conjecture is false (too strong)⁶.

For us the desired modification of data would consist in removing all radiation outside some sphere and to maintain the old data set inside some smaller sphere still containing all the black holes. Their masses, distances etc would then be preserved. Clearly, a sufficient condition (possibly also necessary, if the conjecture mentioned above should indeed be true) for really removing the radiation and obtain a smooth future null infinity \mathcal{I}^+ (at least in a neighbourhood of i_0) is to modify the data outside the larger sphere so as to become *exactly* Schwarzschild (in the time symmetric case).

A priori it is not at all obvious that such a modification exists, as the data have to satisfy the mentioned constraints which are of (underdetermined) elliptic type. Fortunately, such a modification is indeed possible, as was shown in 2000 through a non-constructive existence proof [21]. The pattern of modification is precisely the one envisaged above, where outside a larger sphere one obtains the exterior Schwarzschild data, inside the inner sphere the restriction of the original data set, and in the annular region in between the two spheres one has some interpolating metric that furnishes a smooth transition between the two. The proof in [21] merely asserts the existence of a transition region without further control of its size, and the existence of a transition metric without further control of its properties.

An attempt to make this procedure explicit in the simplest case of the two-hole Brill–Lindquist data was made in [22]. Since these initial data are axisymmetric, the central idea here was to also restrict the transition metric to a simple axisymmetric form of Brill waves [23]. A central concern of [22] was to find out whether this Corvino-like modification of the two-hole Brill–Lindquist data set using Brill waves could be used to reduce the overall ADM energy. This is not obvious since although one clearly removed all gravitational radiation outside the larger sphere, one possibly also re-introduces new one in the transition region, possibly by an inappropriate choice of the transition metric. On the other hand, one suspects

⁶We thank Piotr Chruściel for pointing this out.

on physical grounds that such a reduction of energy should clearly be possible, given the existence of spurious radiation in the first place. Presumably one just has to make the right use of the large freedom in choosing the transition metric to achieve that end, but a clear proof that this is indeed possible was, and still is, missing. In this paper we contribute towards a decision on that question.

Building on ideas of [22] some recent numerical implementation [24, 25] found, somewhat surprisingly, no evidence that an overall mass reduction is indeed possible, though the converse was also not ruled out and the question remained open. As the authors themselves admitted, their approach severely restricted the set of transition metrics, thereby possibly missing out the ‘good ones’. Here we present a novel approach to the numerical implementation that allows to avoid the overdetermined nature of the boundary-value problems encountered in [24, 25]. This will allow a larger flexibility in choosing transition metrics, possibly including energy reducing ones. But that possibility still awaits being turned into reality.

2. The gluing construction

We will start with a short summary of the main statement in [21]. For any smooth, asymptotically flat, and scalar flat metric \hat{g} on \mathbb{R}^n , $n \geq 3$, which is conformally flat at infinity and has positive mass \hat{M} , and any compact set $\mathcal{K} \subset \mathbb{R}^n$, there is a scalar flat metric g on \mathbb{R}^n which is exactly Schwarzschild near infinity yet satisfies $g \equiv \hat{g}$ inside \mathcal{K} . Here, ‘near infinity’ means outside a compact set. In the proof, a candidate metric \tilde{g} is constructed which simply blends smoothly between the interior metric \hat{g} and a Schwarzschild end $g_{M,c}^S$ of ADM mass M and center of mass c ⁷. This blending is confined to an *annular region* $A_R := B_{2R} \setminus \bar{B}_R$, where R is the *gluing radius* and B_R is an open ball of radius R (with respect to the asymptotically flat coordinates). The candidate metric \tilde{g} will then in general not be scalar flat, i.e. we have $R(\tilde{g}) \neq 0$ on A_R . Corvino now proves that for sufficiently large R there exists a mass M , center of mass c , and a smooth deformation h with support on A_R such that $R(\tilde{g} + h) \equiv 0$. Due to the localized nature of the gluing, the proof works for any conformally flat end of a scalar flat asymptotically flat metric \hat{g} , which includes non-trivial black hole data. However, the proof does not indicate how the deformation h or the parameters M and c of the Schwarzschild end can be obtained in practice.

In order to implement such a construction in a concrete case, Giulini and Holzegel [22] glue a Schwarzschild end, i.e. a spacelike $t = \text{const}$ slice of an exterior Schwarzschild metric in isotropic coordinates,

$$g_M^S = (\psi_M^S)^4 \delta := \left(1 + \frac{M}{2\|\mathbf{x}\|}\right)^4 \delta, \quad (2)$$

to a Brill–Lindquist interior metric

$$g^{\text{BL}} = (\psi^{\text{BL}})^4 \delta := \left(1 + \frac{m}{2\|\mathbf{x} - \mathbf{x}_0\|} + \frac{m}{2\|\mathbf{x} + \mathbf{x}_0\|}\right)^4 \delta, \quad (3)$$

where $\mathbf{x}_0 = (0, 0, d/2)^T$ and δ is the flat 3-metric. Equation (3) describes two black holes of equal mass at the moment of time symmetry with positions on the z -axis symmetrical about the coordinate origin, justifying our choice of $c = 0$ for the Schwarzschild end in (2). Note

⁷We recall once more that the ADM mass is a proper geometric invariant of a manifold with end, if the end is asymptotically flat in a suitable sense; see [18]. In case there are more such ends, there is one ADM mass for each end.

that at spatial infinity $\|\mathbf{x}\| \rightarrow \infty$ (2) and (3) have ADM masses M and $2m$, respectively. The metric (3) has two more asymptotically flat ends for $\mathbf{x} \rightarrow \pm\mathbf{x}_0$, the ADM masses of which are equal and given by $m(1 + m/2d)$, which are to be identified with the masses of the individual holes. Hence the overall ADM mass of (3) (at spatial infinity) differs from the sum of the individual ADM masses by the amount $-m^2/d$, which is to be interpreted as the binding energy of the two holes.

Since both g_M^S and g^{BL} have cylindrical symmetry, the initial blending can be performed using a conformally transformed *Brill wave* [23], which is the most general axisymmetric 3-metric. In spherical polar coordinates it reads

$$g_{\text{Brill}} = \psi^4 (e^{2q} (dr^2 + r^2 d\theta^2) + r^2 \sin^2 \theta d\phi^2). \quad (4)$$

Here, ψ and q are functions of r and θ satisfying the following conditions stated in [23]:

$$q = 0 \quad \text{for } \theta = 0 \text{ and } \theta = \pi \text{ (on the } z\text{-axis)}, \quad (5a)$$

$$\frac{\partial q}{\partial \theta} = 0 \quad \text{for } \theta = 0 \text{ and } \theta = \pi \text{ (on the } z\text{-axis)}, \quad (5b)$$

$$q \in \mathcal{O}(r^{-2}) \quad \text{for } r \rightarrow \infty, \quad (5c)$$

and

$$\psi > 0 \quad \text{everywhere}, \quad (6a)$$

$$\psi - 1 \in \mathcal{O}(r^{-1}) \quad \text{for } r \rightarrow \infty, \quad (6b)$$

$$\frac{\partial \psi}{\partial \theta} = 0 \quad \text{for } \theta = 0 \text{ and } \theta = \pi \text{ (on the } z\text{-axis)}. \quad (6c)$$

One possible choice for a conformal factor ψ realizing a smooth blending between g^{BL} and g_M^S would be

$$\psi(r, \theta) = \beta(r, \theta) \psi^{BL}(r, \theta) + (1 - \beta(r, \theta)) \psi_M^S(r), \quad (7)$$

where β is any smooth cutoff function in A_R satisfying

$$\beta(r, \theta) = \begin{cases} 1 & \text{for } r \leq R \\ 0 & \text{for } r \geq 2R, \end{cases} \quad (8a)$$

$$\frac{\partial^n \beta}{\partial r^n} = 0 \quad \text{for all } n \geq 1 \text{ and } r = R \text{ or } r = 2R, \quad (8b)$$

$$\frac{\partial \beta}{\partial \theta} = 0 \quad \text{for } \theta = 0 \text{ and } \theta = \pi. \quad (8c)$$

The first condition ensures that we blend from the Brill–Lindquist to the Schwarzschild conformal factor inside A_R , while the second condition guarantees smoothness of the radial blending. The third condition follows from (6c).

Note that a choice of the form (7) and $q \equiv 0$ just corresponds to a candidate metric \tilde{g} for which, in general, $R(\tilde{g}) \neq 0$ in A_R . However, if we assume the final glued metric $g = \tilde{g} + h$ to preserve the cylindrical symmetry, then it can also be expressed in the form of (4), i.e. $\tilde{g} + h = g_{\text{Brill}}$ for some choice of ψ and q . Inserting now (4) into $R(g_{\text{Brill}}) = 0$, we get

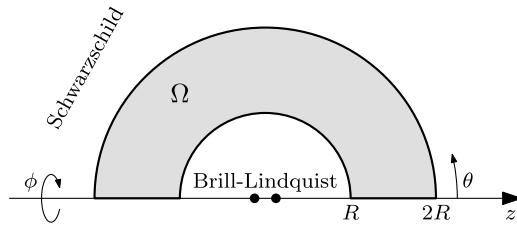


Figure 2. Half annular plane Ω on which to solve equation (10).

$$\begin{aligned} & \left(\frac{\partial^2}{\partial r^2} + \frac{1}{r} \frac{\partial}{\partial r} + \frac{1}{r^2} \frac{\partial^2}{\partial \theta^2} \right) q(r, \theta) \\ &= -4\psi^{-1} \left(\frac{\partial^2}{\partial r^2} + \frac{1}{r} \frac{\partial^2}{\partial \theta^2} + \frac{2}{r} \frac{\partial}{\partial r} + \frac{\cot \theta}{r^2} \frac{\partial}{\partial \theta} \right) \psi(r, \theta), \end{aligned} \quad (9)$$

which can be read as a 2-dimensional Poisson equation for q

$$\Delta^{(2)} q = f := -4 \frac{\Delta^{(3)} \psi}{\psi}. \quad (10)$$

If equation (10) is solved with suitable conditions on q and ψ , the scalar curvature vanishes everywhere and the gluing has been performed.

2.1. Boundary conditions

We require g_{Brill} to be equal to g_M^S for $r \geq 2R$ and g^{BL} for $r \leq R$. This means that $q = 0$ and $\Delta^{(3)} \psi = 0$ outside A_R , thereby trivially satisfying (10). Hence, equation (10) is to be solved on A_R only, which, due to the cylindrical symmetry, reduces to the half annular plane Ω depicted in figure 2. Smoothness of g_{Brill} then implies

$$q = 0 \quad \text{for } r = R \text{ and } r = 2R \text{ (on the radial boundary)}, \quad (11a)$$

$$\frac{\partial^n q}{\partial r^n} = 0 \quad \text{for all } n \geq 1, r = R \text{ and } r = 2R. \quad (11b)$$

For the same reasons, conditions (11) also apply to $\Delta^{(3)} \psi$ and hence to f . Fortunately, this simplifies the conditions for q : if (11) holds for $n = 1$, then by equation (10) it holds for any $n > 1$. Combining this with (5), the complete boundary conditions for q consist of homogeneous Dirichlet and homogeneous Neumann conditions on $\partial\Omega$. Clearly, this makes equation (10) overdetermined since the pure Dirichlet problem on Ω already has a unique solution, see theorem 4.3 in [26]. Therefore, the task is now to find a conformal factor ψ blending smoothly from ψ^{BL} to ψ_M^S such that (10) has a solution q satisfying Dirichlet and Neumann conditions. In [22] this is called the DN-problem and a solution q a DN-solution.

3. The numerical strategy

An analytical treatment of the DN-problem has been carried out in [22] where an approximation result could be obtained. The objective of the present paper is to present a strategy for numerically approximating DN-solutions and find explicit values of the glued Schwarzschild mass M .

3.1. Previous results

The first step towards a numerical solution has been made by Doulis and Rinne in [24] and [25] and the strategy here extends and corrects their results. Specifically, Doulis and Rinne employ a numerical method to find a mass M and a gluing function β based on iteratively solving problems that are still overdetermined, i.e. in each step they impose a Neumann condition on $\partial\Omega$ and additionally a Dirichlet condition on the *arches* at $r = R$ and $r = 2R$. With these boundary conditions, the Poisson equation (10) has no solution on Ω in general; see section 2.1.

To determine whether it is still possible that the numerical search converges to an existing solution, Doulis and Rinne carry out convergence tests on their results. Since the solutions are computed using a pseudospectral method, the expected behaviour is exponential convergence of the numerical solutions to the exact solution for increasing resolution. An approximation of the error of a particular numerical solution is given by the last coefficient of the expansion of the solution into the chosen basis functions [27]. This argument applies to one-dimensional problems. For higher dimensions, one typically chooses a particular basis set for each dimension and expands the solution into the tensor product basis. The coefficients of solutions of two-dimensional problems then become a matrix (a_{kl}) , $k = 0, \dots, K$, $l = 0, \dots, L$, where K and L define the resolution, i.e. the number of basis functions to consider. The question now is how to approximate the error using the ‘last coefficient’ in case of a coefficient matrix. In [25], Doulis and Rinne choose a_{KL} and plot how it decays exponentially in K when increasing K and L at the same time. They also plot how the L^2 -norm of the difference between lower resolution solutions and a reference solution of high resolution decays.

We were able to reproduce this strategy and obtained very similar results at the resolutions mentioned in [25]; see figure 3. Even though we can closely match the convergence of the a_{KL} coefficient (figure 4(a)), we observe poor convergence of the coefficient a_{K0} , i.e. in the radial direction, especially at higher resolutions (figure 4(b))⁸. Furthermore, the conformal factor ψ numerically determined in this process does not pass the criterion of equation (13) developed in the following subsection. In light of these results, we were not able to confirm that the numerical strategy presented in [25] successfully produces DN-solutions.

3.2. Our strategy

The basic idea here is as follows. An ansatz of the form (7) is perturbed by a function $\chi(r, \theta)$, i.e.

$$\psi(r, \theta) = \beta(r, \theta) \psi^{\text{BL}}(r, \theta) + (1 - \beta(r, \theta)) \psi_M^{\text{S}}(r) + \chi(r, \theta), \quad (12)$$

such that the DN-problem is solvable. This latter condition is tested by *decomposing* the full DN-problem into two problems, each having an existing and unique solution. The first problem is obtained by taking (10) and imposing a Dirichlet condition just on the arches, and a Neumann condition just on the z -axis for $\theta = 0$ and $\theta = \pi$. This problem is uniquely solvable (see e.g. remark 2.1 in [28]) and we will call its solution a dn-solution q_{dn} . The second problem is obtained by exchanging the boundary conditions and imposing a Neumann condition on the arches and a Dirichlet condition on the z -axis. Solutions of this problem will be called nd-solutions q_{nd} . If, for some particular χ and M , we have

⁸The cause is most likely the very wide bump-type function, which is constructed with $b_1 = b_2 = 10^{-2}$, see equation (3.2) in [25]. At low radial resolutions, the collocation points do not sample this function and its derivatives sufficiently fine enough, such that the Neumann condition is effectively ignored.

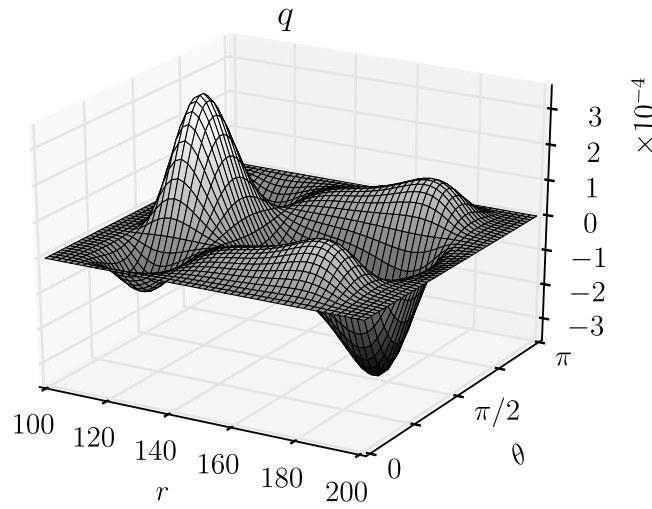


Figure 3. Result of our implementation of the strategy of Doulis and Rinne corresponding to the case of figure 6(b) in [25] (i.e. $m = 2$, $d = 10$, $R = 100$). Shown is the numerical solution q of the Poisson problem (10) after the gluing function $\beta(r, \theta)$ had been determined as in [25] at the same numerical resolution of $K = L = 25$. The found ADM mass is $M = 4.000\,027\,17$.

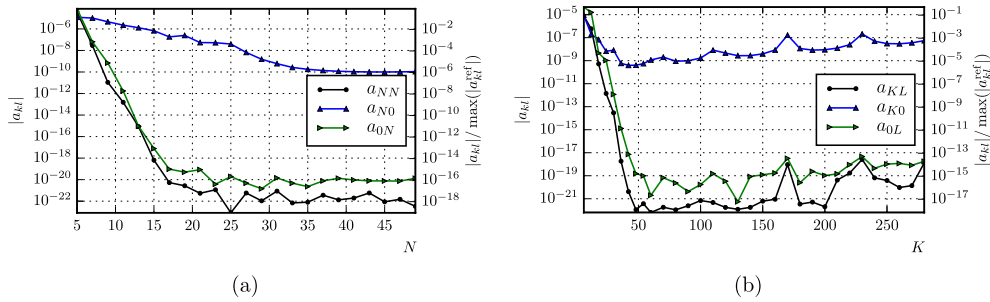


Figure 4. Convergence of three different choices of a ‘last coefficient’ for numerical resolutions of (a) $K = L = N$ and (b) $L = \lfloor K/3 \rfloor$ (i.e. the integer part of $K/3$). As explained in section 3.3, the $\pi/2$ -symmetry effectively removes half of the coefficients in the angular ‘direction’, leaving in the end $\lfloor K/2 \rfloor$ significant angular coefficients for case (a) and $\lfloor K/6 \rfloor$ for (b). The scale on the right of each plot is normalized with respect to the largest coefficient of the solution of highest resolution. As can clearly be seen in both cases, the coefficient a_{KL} converges most rapidly and does not reflect the fact that we have poor convergence in the radial direction. Since the values of the a_{K0} curve in (b) are far away from the floating point roundoff plateau, one may question convergence and instead assume that at the higher radial resolutions, the very wide bump-type function used in [25] starts to get sampled fine enough such that the overdeterminedness of the equation begins to show an effect.

$$q_{\text{dn}} \equiv q_{\text{nd}}, \tag{13}$$

then both solutions satisfy Dirichlet and Neumann conditions on $\partial\Omega$ and hence solve the DN-problem. On the other hand, if (13) is not satisfied, then equation (10) has no DN-solution.

Naturally, the conditions to impose on χ are directly related to those of ψ . Specifically, we require $\partial\chi/\partial\theta = 0$ on the z -axis and that χ be of bump-type in the radial direction, i.e. $\partial^n\chi/\partial r^n = 0$ for all $n \geq 0$ on the arches.

We still have to consider that the ADM mass M of the glued Schwarzschild end cannot be chosen arbitrarily—Corvino [21] just proves that there exists a mass such that the gluing can be done. This fact manifests itself in the current construction as follows. The DN-solution will also be a pure Neumann solution of the Poisson problem. But for such a solution to exist, the *compatibility condition*

$$\int_{\Omega} f \, d^3x = 0 \quad (14)$$

has to be satisfied, as can easily be seen when integrating equation (10) over Ω and using Gauss's theorem on the left-hand side. Note that the mass M enters the inhomogeneity f through ψ_M^S in the ansatz (12). We therefore read (14) as a condition for M . In [25], Doulis and Rinne obtain an equivalent condition,

$$M = \int_0^\pi \int_0^\infty \left[\left(\frac{\partial_r \psi}{\psi} \right)^2 + \left(\frac{\partial_\theta \psi}{r\psi} \right)^2 \right] r^2 \sin \theta \, dr \, d\theta, \quad (15)$$

which they call the *integrability condition*. Again, equation (15) is not an identity, since the mass also enters the integrand through ψ . As this condition is necessary for a Neumann solution to exist, there can be no choice of χ leading to a DN-solution unless it is satisfied.

3.3. Numerical setup

Mathematically, the task is to find a ‘root’ of the map $(\chi, M) \mapsto q_{\text{dn}} - q_{\text{nd}}$. To guarantee the bump-condition for χ , we use the ansatz

$$\chi(r, \theta) = B_\chi(r) \hat{\chi}(r, \theta), \quad (16)$$

where B_χ is a bump-type function of the form

$$B(r) := \text{sech}(s(r)), \quad s(r) := \frac{R}{2} \left(\frac{b_1}{r-2R} + \frac{b_2}{r-R} \right), \quad (17)$$

for some $b_1, b_2 > 0$. For $\hat{\chi}$ we use a truncated expansion into a product basis of Chebyshev polynomials T_n and cosines,

$$\hat{\chi}(r, \theta) = \sum_{i=0}^{N_r} \sum_{j=0}^{N_\theta-1} a_{ij}^\chi T_i(x(r)) \cos(2j\theta). \quad (18)$$

Here, the linear map $x : [R, 2R] \rightarrow [-1, 1]$,

$$x(r) = \frac{2}{R}r - 3, \quad (19)$$

is used to transform the problem to the domain of the Chebyshev polynomials and the cosines are used to impose $\partial\chi/\partial\theta = 0$ on the z -axis. We choose just the even cosine frequencies due to the $\pi/2$ -symmetry of the whole problem resulting from the choice of equal masses of the two Brill–Lindquist black holes.

Using (18) to define $\hat{\chi}$ means that we have $N = (N_r + 1)N_\theta$ degrees of freedom, which can be used to either control the coefficients a_{ij}^χ directly, or to specify values $\hat{\chi}$ should have at, for example, the N different Gauss–Lobatto collocation points $(r(x_i), \theta_j)$, where $r(x)$ is the inverse of (19) and

$$\begin{aligned} x_i &= \cos\left(\frac{\pi i}{N_r}\right), & i &= 0, \dots, N_r, \\ \theta_j &= \frac{\pi j}{2N_\theta}, & j &= 0, \dots, N_\theta - 1. \end{aligned} \quad (20)$$

For a particular χ , we numerically compute M by finding the smallest value $M > 0$ satisfying the integrability condition (15).

Finally, we need to have highly accurate numerical solutions for q_{dn} and q_{nd} in order to evaluate their difference. Similar to [25], we choose the pseudospectral method [27, 29] and expand the two solutions into Chebyshev polynomials for both r and θ

$$\begin{aligned} q_{\text{nd}}(r, \theta) &= \sum_{i=0}^{N_r^q} \sum_{j=0}^{N_\theta^q} a_{ij}^{\text{dn}} T_i(x(r)) T_{2j}(y(\theta)), \\ q_{\text{dn}}(r, \theta) &= \sum_{i=0}^{N_r^q} \sum_{j=0}^{N_\theta^q} a_{ij}^{\text{nd}} T_i(x(r)) T_{2j}(y(\theta)), \end{aligned} \quad (21)$$

where the resolution N_r^q, N_θ^q is independent of the resolution N_r, N_θ of $\hat{\chi}$. Here, $y(\theta) := 2\theta/\pi - 1$ transforms the angular range to the domain of the Chebyshev polynomials and we have used only the even polynomials to accommodate the $\pi/2$ -symmetry. By choosing Chebyshev polynomials for the angular ‘direction’, we have the required freedom to impose any kind of boundary condition on the z -axis. For the dn- and nd-problems, all boundary conditions are imposed in the standard way by replacing rows in the resulting pseudospectral matrix equation. Again, we use Gauss–Lobatto points for x and also for y , for which they reduce to

$$y_j = \cos\left(\frac{\pi j}{2N_\theta^q}\right), \quad j = 0, \dots, N_\theta^q. \quad (22)$$

3.4. The root search

The search for χ and M is carried out as follows. Let $\mathbf{v} \in \mathbb{R}^N$ be the vector encoding the N degrees of freedom of $\hat{\chi}$, e.g. by specifying the values of $\hat{\chi}$ on the grid (20) of Gauss–Lobatto points. This is transformed to spectral space providing the coefficients a_{ij}^χ . With χ fixed, we use the integrability condition (15) to determine M . In case no such mass exists (there are cases in which (15) cannot be satisfied by any M), the search cannot continue at this point, but this usually only occurs for too small gluing radii R . With χ and M , we can evaluate the inhomogeneity f of the Poisson equation (10) and compute the two solutions q_{dn} and q_{nd} with the pseudospectral method. Sampling the difference $q_{\text{dn}} - q_{\text{nd}}$ on the Gauss–Lobatto grid of $\hat{\chi}$ results in N values which constitute the vector $\mathbf{w} \in \mathbb{R}^N$. Note that this defines a map $F : \mathbb{R}^N \rightarrow \mathbb{R}^N$, $\mathbf{v} \mapsto \mathbf{w}$.

Let ε be the greater of the two absolute errors of q_{dn} and q_{nd} , i.e.

$$\varepsilon := \max\{\|q_{\text{dn}} - q_{\text{dn}}^{\text{exact}}\|_\infty, \|q_{\text{nd}} - q_{\text{nd}}^{\text{exact}}\|_\infty\}. \quad (23)$$

We consider \mathbf{v}^* to be an approximate root of F if $\|F(\mathbf{v}^*)\|_\infty \lesssim \varepsilon$. Recall that the resolution N_r, N_θ of $\hat{\chi}$ also controls the grid on which $q_{\text{dn}} - q_{\text{nd}}$ is measured. If this resolution is high enough, we will have $\|F(\mathbf{v}^*)\|_\infty \approx \|q_{\text{dn}} - q_{\text{nd}}\|_\infty$ and hence

$$\|q_{\text{dn}} - q_{\text{nd}}\|_\infty \lesssim \varepsilon. \quad (24)$$

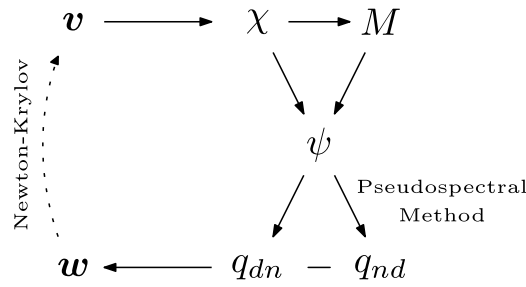


Figure 5. Diagram showing the numerical strategy for finding a DN-solution.

If condition (24) is satisfied, we cannot determine—at least at the chosen resolution N_r^q, N_θ^q of the pseudospectral solutions—whether there is any difference between q_{dn} and q_{nd} . We will then call them identical, thus a DN-solution, within the numerical limits. Naturally, one aims to choose the highest feasible resolution N_r^q, N_θ^q in order to obtain a low value of ε .

To find a root v^* of F , we use an approximate Newton search, the *Newton–Krylov* algorithm [30], which is suitable for high-dimensional problems. Figure 5 shows the basic scheme of the numerical strategy. In order to enable the Newton–Krylov search to succeed, it turned out that we had to employ means to avoid high-order contributions in the expansion of $\hat{\chi}$ at the beginning of the search. This is accomplished by starting with a low resolution for $\hat{\chi}$ and applying a low-pass filter, i.e. effectively damping the coefficients a_{ij}^χ for higher i, j . In successive Newton–Krylov runs, each taking only one approximated Newton step, the resolution of $\hat{\chi}$ and the dimension of the Krylov-subspace are increased and the damping reduced until the target configuration is reached. At this point, the Newton–Krylov algorithm takes as many steps as required to satisfy condition (24).

Most of the code implementing this strategy has been written from scratch in Python including the pseudospectral method. Library routines of SciPy [31], NumPy [32], and mpmath [33] were used for the root finding, integration, and matrix equation solving.

3.5. Testing the convergence on an exact solution

A crucial aspect of the above strategy is to obtain both a high accuracy and a good estimation of the error ε of the pseudospectral solutions q_{dn} and q_{nd} . The first of these goals is achieved by choosing a sufficiently high resolution N_r^q, N_θ^q , while for the second goal we employ a detailed convergence analysis and compare the solutions with a known exact solution of a very similar problem. Such a test problem is provided by the analytical solution for an approximated inhomogeneity f obtained in [22]. For the case $M = 2m$, an explicit solution formula can be given. To this end, consider the ansatz (7) for ψ and choose β as

$$\beta(r, \theta) = \alpha(r) + \mu(r) \sin^2 \theta, \quad (25)$$

where α satisfies (8a) and (8b) and μ is of bump-type. Expanding now the inhomogeneity in the inverse gluing radius R up to first order, Giulini and Holzegel obtain an ordinary differential equation for μ and conditions for α . For $M = 2m$, the result can be written as (see [34])

$$\int_R^{2R} t^{-(2-\sqrt{3})} \alpha'(t) dt = 0, \quad \int_R^{2R} t^{-(2+\sqrt{3})} \alpha'(t) dt = 0, \quad (26a)$$

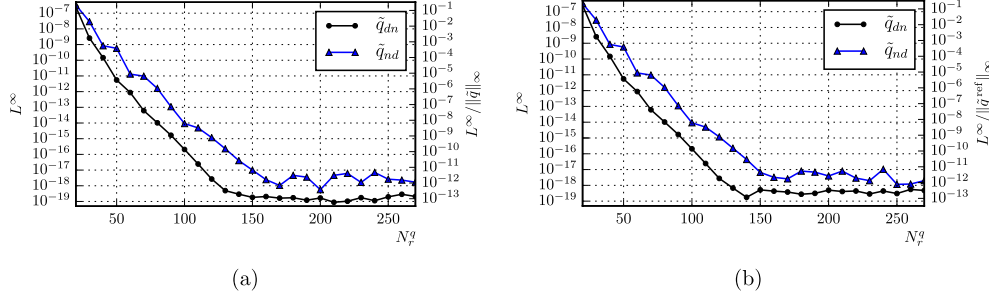


Figure 6. Convergence of the pseudospectral solutions \tilde{q}_{dn} and \tilde{q}_{nd} to the exact solution \tilde{q} in (a) and to the solutions $\tilde{q}_{dn}^{\text{ref}}$ and $\tilde{q}_{nd}^{\text{ref}}$, respectively, in (b). The reference solutions for (b) were computed with a resolution of $N_r^q = 280$. For all solutions, we chose N_θ^q to be the integer part of $N_r^q/6$. The following parameters were used: $d = 10$, $m = 2$, $M = 2m = 4$, $R = 5000$, and $b_1 = b_2 = 2$ for both α_0 and B_α .

$$\mu(r) = -\frac{1}{2}r^2\alpha''(r) + \frac{3}{2}r\alpha'(r) + \int_R^r \alpha'(t) \left(\frac{3+2\sqrt{3}}{2} \left(\frac{r}{t}\right)^{2-\sqrt{3}} + \frac{3-2\sqrt{3}}{2} \left(\frac{r}{t}\right)^{2+\sqrt{3}} \right) dt. \quad (26b)$$

To satisfy the conditions (26a) for α we choose

$$\alpha(r) = \alpha_0(r) + B_\alpha(r)(c_0 + c_1r), \quad (27)$$

where B_α is a bump-type function of the form (17) and α_0 is given by

$$\alpha_0(r) := \frac{1}{2}(1 + \tanh(s(r))). \quad (28)$$

The constants c_0, c_1 are found via a simple Newton search for a root of the map $(c_0, c_1) \mapsto (I_1, I_2)$, where I_1, I_2 are the numerical values of the integrals in (26a). Using the results of [22], one can then easily write down the exact solution \tilde{q} of the approximated problem in terms of α and μ . Note that \tilde{q} is a DN-solution and that we therefore expect the pseudospectral solutions \tilde{q}_{dn} and \tilde{q}_{nd} of this approximated problem to coincide.

Figure 6 shows that this is in fact the case up to a remaining roundoff error of about 10^{-17} and that the convergence for increasing resolution is exponential as would be expected. It also exhibits the typical roundoff plateau which occurs when the floating point errors dominate. Note that figure 6(b) provides a very good estimate of the accuracy despite being a purely intrinsic test without knowledge of the exact solution \tilde{q} of the approximated DN-problem.

4. Numerical results

Here we present numerical results for the non-approximated DN-problem. Starting the search for χ and M with the ansatz (12) for ψ and choosing $\beta(r, \theta) = \alpha_0(r)$ as in (28) with $b_1 = b_2 = 2$ and the configuration $d = 10$, $m = 2$, and $R = 5000$, we obtain a solution for the deformation χ depicted in figure 7(a). During the search, the resolution for the pseudospectral solutions has been chosen to be $N_r^q = 160$, $N_\theta^q = 26$. Figure 7(b) shows the dn-solution q_{dn} , which is close to the nd-solution q_{nd} with $\|q_{dn} - q_{nd}\|_\infty \approx 2.4 \times 10^{-19}$. This is compatible

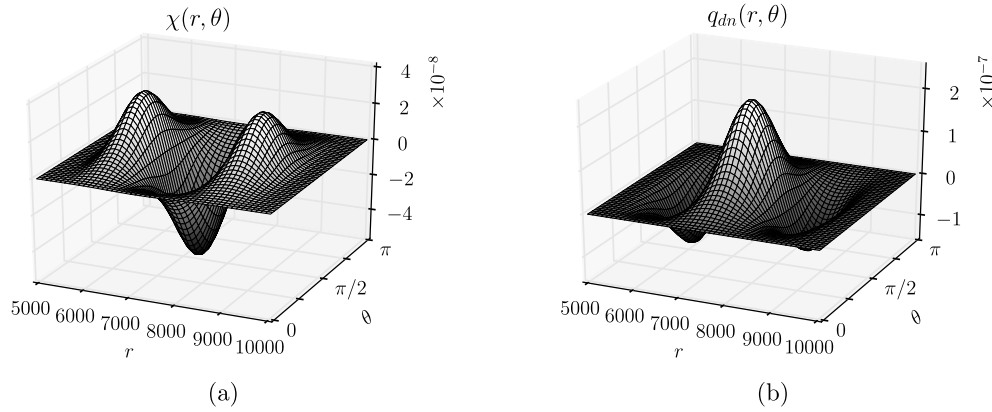


Figure 7. Solution of the numerical search for χ depicted in (a). In (b), the dn-solution is shown which is equal to the nd-solution within the numerical limits.

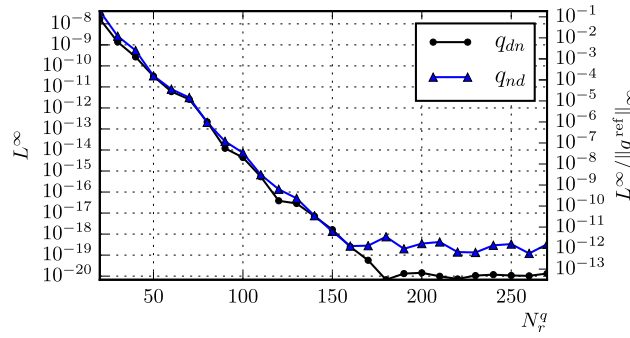


Figure 8. Convergence of the dn- and nd-solutions to the reference solutions q_{nd}^{ref} and q_{dn}^{ref} , respectively, computed with $N_r^q = 280$, $N_\theta^q = 46$.

with the accuracy read off from figure 8 such that condition (24) is satisfied and therefore provides a strong indication that this solution is close to an exact solution of the DN-problem. The ADM mass M of the glued Schwarzschild end in this result reads

$$M = 2m + (7.5620 \pm 0.0001) \times 10^{-10}. \quad (29)$$

Using the same interior configuration m , d , and gluing radius R , but different search parameters (initial resolution for $\hat{\chi}$, etc), we were able to find different combinations of deformations χ and ADM masses M which still satisfy the condition (24). The masses found thus far range from about $2m + 1.8 \times 10^{-11}$ to $2m + 4.7 \times 10^{-8}$. We emphasize that these different masses were glued with the exact same gluing radius R . Studying the dependency of this glued mass on the gluing radius as done in [25] therefore seems not to be reasonable in our case, as it is unclear how the specifics of the solution strategy enter the distribution of the masses we find.

5. Conclusion

The above results provide strong indication that the presented numerical strategy is able to successfully produce a highly accurate gluing of a Brill–Lindquist interior to the exterior

Schwarzschild metric, so as to everywhere satisfy the time-symmetric vacuum constraints. Moreover, the way this strategy is set up leaves a large freedom for how the final gluing is done. As this freedom is a genuine feature of Corvino's construction [21], it should clearly be preserved, at least to some extent, in any more or less faithful numerical implementation, like the one presented here. This freedom then opens up the possibility to impose further conditions on the gluing, depending on the desired properties one wishes the final metric to share. One such property, that we already used as motivation in the introduction, is the minimisation of the ADM mass of the glued Schwarzschild end. Such a minimisation is taken to signal the removal of spurious gravitational radiation. On the other hand, it seems clear that just picking *some* gluing function will generically add rather than subtract gravitational waves and hence result in overall masses $M > 2m$, as we have seen above and as was also seen in [25]. But, as shown in our paper, numerical implementations exist which preserve the freedom of Corvino's construction to a large extent and which may eventually be used to adjust the gluing so as to actually reduce the overall mass M below $2m$. Presently we do not know how to effectively translate such an energy-minimisation condition into the numerical strategy in a systematic (i.e. not just based on trial and error) way, but our work suggests that this should be possible. Looking further ahead we mention that the original gluing construction, devised in [21], can be generalised to non time-symmetric data representing spinning black holes. This has been shown in [35], where the exterior metric one glues onto is now a slice of Kerr spacetime. This may eventually help in gaining proper analytic understanding of how to remove spurious radiation in the physically most relevant cases, that of binary systems with orbital and spin angular momenta. But we believe that before that more difficult problem can be attacked one should seriously try to first gain a decent analytic understanding of the admittedly idealised situation investigated here.

Last, but not least, we mention that quite independently of the question of mass reduction, Corvino-type gluing constructions may generally find interesting applications in numerical evolution codes. Being exactly Schwarzschild in a neighbourhood of spatial infinity, smooth null infinities \mathcal{I}^+ are guaranteed. This allows evolutions of hyperboloidal slices extending to \mathcal{I}^+ , which in turn enable unambiguous extractions of gravitational radiation data. A detailed description of such a scheme is provided by Doulis and Rinne in [25].

ORCID iDs

Domenico Giulini  <https://orcid.org/0000-0003-3123-7257>

References

- [1] Abbott B P *et al* 2016 Observation of gravitational waves from a binary black hole merger *Phys. Rev. Lett.* **116** 061102
- [2] Abbott B P *et al* 2017 GW170608: observation of a 19 solar-mass binary black hole coalescence *Astrophys. J. Lett.* **851** L35
- [3] Abbott B P *et al* 2017 GW170814: a three-detector observation of gravitational waves from a binary black hole coalescence *Phys. Rev. Lett.* **119** 141101
- [4] Abbott B P *et al* 2017 GW170817: observation of gravitational waves from a binary neutron star inspiral *Phys. Rev. Lett.* **119** 161101
- [5] Giulini D 2014 Dynamical and Hamiltonian formulation of general relativity *Springer Handbook of Spacetime* ed A Ashtekar and V Petkov (Berlin: Springer) pp 323–62 (extended version (76 pages) at arXiv:1505.01403)
- [6] Brill D R and Lindquist R W 1963 Interaction energy in geometrostatics *Phys. Rev.* **131** 471

- [7] Giulini D 1998 On the construction of time-symmetric black hole initial data *Black Holes: Theory and Observation (Lecture Notes in Physics vol 514)* ed F W Hehl *et al* (Berlin: Springer) pp 224–43
- [8] Bowen J M and York J W Jr 1980 Time-asymmetric initial data for black holes and black-hole collisions *Phys. Rev. D* **21** 2047–56
- [9] Brandt S and Brüggmann B 1997 A simple construction of initial data for multiple black holes *Phys. Rev. Lett.* **78** 3606–9
- [10]ourgoulhon É 2012 *3 + 1 Formalism in General Relativity (Lecture Notes in Physics vol 846)* (Berlin: Springer)
- [11] Cook G B 2000 Initial data for numerical relativity *Living Rev. Relativ.* **3** 5
- [12] Spherhake U 2007 Binary black-hole evolutions of excision and puncture data *Phys. Rev. D* **76** 104015
- [13] Dain S, Lousto C O and Takahashi R 2002 New conformally flat initial data for spinning black holes *Phys. Rev. D* **65** 104038
- [14] Lovelace G 2009 Reducing spurious gravitational radiation in binary-black-hole simulations by using conformally curved initial data *Class. Quantum Grav.* **26** 114002
- [15] Mösta P, Andersson L, Metzger J, Szilágyi B and Winicour J 2015 The merger of small and large black holes *Class. Quantum Grav.* **32** 235003
- [16] Valiente Kroon J A 2003 Early radiative properties of the developments of time-symmetric conformally flat initial data *Class. Quantum Grav.* **20** L53–9
- [17] Newman T and Penrose R 1965 10 exact gravitationally-conserved quantities *Phys. Rev. Lett.* **15** 231–2
- [18] Bartnik R 1986 The mass of an asymptotically flat manifold *Commun. Pure Appl. Math.* **39** 661–93
- [19] Valiente Kroon J A 2004 A new class of obstructions to the smoothness of null infinity *Commun. Math. Phys.* **244** 133–56
- [20] Hintz P and Vasy A 2017 A global analysis proof of the stability of Minkowski space and the polyhomogeneity of the metric (arXiv:1711.00195)
- [21] Corvino J 2000 Scalar curvature deformation and a gluing construction for the einstein constraint equations *Commun. Math. Phys.* **214** 137–89
- [22] Giulini D and Holzegel G 2005 Corvino’s construction using Brill waves (arXiv:gr-qc/0508070)
- [23] Brill D R 1959 On the positive definite mass of the Bondi–Weber–Wheeler time-symmetric gravitational waves *Ann. Phys.* **7** 466–83
- [24] Doulis G and Rinne O 2015 Numerical Brill–Lindquist initial data with a Schwarzschildian end at spatial infinity *J. Phys.: Conf. Ser.* **600** 012039
- [25] Doulis G and Rinne O 2016 Numerical construction of initial data for Einstein’s equations with static extension to space-like infinity *Class. Quantum Grav.* **33** 075014
- [26] Gilbarg D and Trudinger N S 2001 *Elliptic Partial Differential Equations of Second Order* (Berlin: Springer)
- [27] Boyd J P 2001 *Chebyshev and Fourier Spectral Methods* 2nd edn (New York: Dover)
- [28] Korotov S 2007 Two-sided *a posteriori* error estimates for linear elliptic problems with mixed boundary conditions *Appl. Math.* **52** 235–49
- [29] Canuto C, Hussaini M Y, Quarteroni A and Zang T A 2006 *Spectral Methods: Fundamentals in Single Domains* (Berlin: Springer)
- [30] Knoll D A and Keyes D E 2004 Jacobian-free Newton–Krylov methods: a survey of approaches and applications *J. Comput. Phys.* **193** 357–97
- [31] Jones E *et al* 2001 SciPy: open source scientific tools for Python (<http://www.scipy.org/>) (Accessed: 09 March 2018)
- [32] Walt S V D, Colbert S C and Varoquaux G 2011 The numpy array: a structure for efficient numerical computation *Comput. Sci. Eng.* **13** 22–30
- [33] Johansson F *et al* 2018 mpmath: a Python library for arbitrary-precision floating-point arithmetic (version 0.19) (<http://mpmath.org/>)
- [34] Pook-Kolb D 2018 Numerical construction of corvino-type gluing for Brill–Lindquist initial data *Master’s Thesis* Leibniz Universität Hannover
- [35] Corvino J and Schoen R M 2006 On the asymptotics for the vacuum einstein constraint equations *J. Differ. Geom.* **73** 185–217